Supporting Information

SI Material and Methods

Phytoplankton abundance and composition. Continuous underway measurements of picophytoplankton abundance and cell size were made using SeaFlow (1). The instrument was equipped with a 457-nm 300-mW laser (Melles Griot). Forward light scatter (a proxy for cell size), red and orange fluorescence were collected using a 457–50 bandpass filter, 572–27 bandpass filter and 692–40 band-pass filter, respectively. Seawater was prefiltered through a 100-µm stainless steel mesh (to eliminate large particles) prior to analysis. The flow rate of the water stream was set at 15 mL min^{-1} through a 200-µm nozzle for both cruises and for the laboratory experiments; this corresponded to an analysis rate of 15 µL min^{-1} by the instrument. A programmable syringe pump (Cavro XP3000, Hamilton Company) continuously injected fluorescent microspheres (1 µm, Polysciences) into the water stream as an internal standard. Data files were created every three minutes, yielding a sampling resolution along the cruise track of 1 km (for a ship cruising at ~11 knots). Field data were analyzed using the R packages *flowPhyto* (2) version 2.4.1, which uses statistical clustering methods to discriminate between different phytoplankton populations, namely *Prochlorococcus*, *Synechococcus* and picoeukaryotes. The R package is available on GitHub (https://github.com/armbrustlab/flowPhyto). Hourly-averaged cell abundances were obtained by calculating the mean of the cell abundances collected every 3-minutes over each 1-hr period (n=20).

Relationship between forward-angle light scatter and cell volume. We estimated the *Prochlorococcus* cell volume using an empirical relationship between light scatter measured by Sea-

1

Flow and cell volume measured by a Coulter Counter for different exponentially growing phytoplankton cultures of cell sizes ranging from 1 to 10 μm, namely *Synechococcus* (WH6501 and WH8201), *Phaeodactylum tricornutum, Emiliana huxleyi, Thalassosira pseudonana, Rhodomonas sp.* and *Geminifera cryophila,* (ordered by increasing cell size). A two-degree polynomial function explained 99% of the variance between forward-angle light scattering (FALS) and cell volume (V):

$$log(V) = 0.546 \times log(FALS)^2 + 1.871 \times log(FALS) + 1.077 \qquad \text{[S1]}$$
($R^2 = 0.996$, $p < 0.001$, n=22)

Prochlorococcus cell volume was below the detection limit of the Coulter Counter, so we were unable to directly measure *Prochlorococcus* cell sizes to calibrate FALS in that size range. Since the empirical polynomial function (equation 1) cannot be extrapolated, we fit a linear relationship to laboratory calibrations between *Synechococcus* FALS and V, assuming the same relationship between FALS and V for *Synechococcus* and *Prochlorococcus* cells:

$$log(V) = 0.524 \times log(FALS) + 0.283 \qquad \text{[S2]}$$
($R^2 = 0.99$, $p < 0.001$, n=8)

We found that FALS was proportional to 5.7 power of the diameter ($d^{5.7}$), which is in good agreement with the prediction from the Mie light scattering theory for picoplankton cells (d^6). This regression equation was used to estimate mean cell volume of *Prochlorococcus* in the field.

Size-based estimates of division rate. We used a size-structured matrix population model developed by Sosik *et al.* (3) to estimate population division rates of *Prochlorococcus*. We implemented Sosik's original Matlab model in an R package *ssPopModel* version 0.1.1, available on Github (https://github.com/armbrustlab/ssPopModel). The model is based on the assumptions

2

that 1) cell growth is determined by light exposure, with other abiotic factors such as nutrient availability and temperature operating at longer time scales, 2) the probability of a cell dividing depends on size, 3) all cells within a discrete size class have the same probability to change to another size class, and 4) a cell divides into two daughter cells, each half the size of the mother cell. The model predicts the cell size distribution over the course of the day using the cell size/cell division relationships and the light-dependence of cell division. Note that the model does not take into account intrinsic cell death. Intrinsic cell death will only affect the estimate of division rate if the probability of cell death varies among the different size classes of *Prochlorococcus*. This has not yet been observed in the field or in cultures. In our study, cell death of *Prochlorococcus* grown in cultures was low (< less than 1%) during the 30-h experiment (Fig. S1B). For these reasons, we did not implement intrinsic death in the size-based division rate model.

First, the measured size distribution is divided equally on a logarithmic scale of base 2. A projection matrix gives the fraction of cells in size class *j* at time *t* that become cells in size class *i* at time *t+dt*. Since the model allows a cell to undergo only one transition from one size to another, *dt* must be low. We set *dt* =10, similar to the original model, so that this is a reasonable assumption.

Each size class can have three potential transitions: growth, cell division or stasis, assuming that intrinsic cell death is negligible. The probability of cell division *d(t)* increases as a power of cell volume (v_i):

$$d(t) = \frac{(av_i)^b}{1+(av_i)^b} dmax \qquad\qquad\qquad \text{[S3]}$$

3

where d_{max} represents the maximum fraction of cells that can divide each time step, and a and b are two constants. Of the cells that do not divide during the time step, a fraction enlarges into the next size class. The probability to grow $g(t)$ depends on the incident radiations $E(t)$ as:

$$g(t) = \left\{ 1 - exp\left[\frac{-E(t)}{E^*}\right]\right\} gmax \qquad \textbf{[S4]}$$

where g_{max} represents the maximum fraction of cells that can grow each time step. Cells in the largest size class do not grow. The cells that do not divide or grow fast enough to reach the next size class during the time step remain in the same size class (i.e. stasis). The probability of stasis $s(t)$ is calculated as:

$$s(t) = 1 - d(t) - g(t) \qquad \textbf{[S5]}$$

The model therefore uses 5 parameters, a, b, d_{max}, E^* and g_{max}. To estimate these parameters, the model is fitted to hourly observations of the number of cells in each size class during a 24-hr period. The projected size distribution at time $t+1$ hr is calculated from the observed distribution at time t by matrix multiplication (using $dt = 10$), where the fraction of cells in each size class is based on the formulas for cell growth, cell division and stasis. The parameters are chosen by minimizing the weighted sum of the squared deviations between the observed and projected hourly size distributions, assuming that the parameters remain constant within a day but may change from day to day. The result of the optimization is a best-fitting, hourly projection matrix and an estimated hourly division rate for each hour of the 24-hr period. We used a 1-hr rolling window to determine the start of each 24-hr period in the time series. We therefore obtained 24 series of hourly projected size distribution and best-fitting parameters for each day.

The model of Sosik *et al.* (3) was developed to estimate *Synechococcus* division rates. A few modifications were necessary in order to produce a better representation of the observed *Prochlorococcus* size distributions. First, the original model does not allow cells to divide during the

4

first 6 hr after dawn to be in agreement with previous observations of natural and cultured *Syn-echocococus*. Our model was modified to allow *Prochlorococcus* cells to divide at any time of the day since in our case cells in G2 phase of the cell cycle were observed throughout the day (Fig. S2 and S3). Second, the original model was recently modified to accommodate bimodal size distributions (4), which is observed in *Synechococcus* in both cultured isolates and natural populations. We did not implement this modification in our model since only unimodal size distributions were observed for *Prochlorococcus* (Fig. S7A, B). Third, the original model uses a least squares approach for parameter optimization. While the least squares method is computationally efficient, it is sensitive to the choice of the initial values of the parameters. We found that the parameters did not converge properly if the parameter values were close to the boundary of the parameter space, which was often the case. In the most recent implementation of this model, Hunter-Cevera *et al.* (4) replaced the least squares approach with a maximum likelihood approach. We instead used a differential evolution algorithm, available from the R package *Deoptim* (5), that was well-suited to this type of problem. We simulated artificial size distributions using 600 random values of the five parameters, subjected to the following constraints $0 < d_{max} < 1$; $0 < g_{max} < 1$; $a > 0$; $b > 0$; $10 < E^* < 2000$, with E^* measured in μE m^{-2} s^{-1}. We found that the optimization was excellent, with best-fitting parameters showing > 96% accuracy with the true set of parameters.

Matrix population models assume that changes in size distributions are only related to cell growth and division. We assumed that there was no differential mortality of *Prochlorococcus* based on cell size. Division rate estimates of *Synechococcus* using the size-structured matrix population model have been shown to be similar between undiluted incubations (higher grazing pressure) and diluted incubations (lower grazing pressure) (4), supporting the assumption that

size-selective grazing is not important. During the northward cruise to California on day 3, as the ship entered more mesotrophic, coastal waters, a three-fold increase in *Prochlorococcus* cell size was observed (Fig. S7A), which is too high to be attributed solely to cell growth and likely reflect increases in cell size due to higher nutrient cell content (12). Our estimates of hourly division rates on day 3 are likely not reliable.

To establish the accuracy of size distribution-based division rate estimates (using SeaFlow measurements of forward-angle light scattering), we compared size-based estimates of *Prochlorococcus* division rates (h^{-1}) with rates of changes in cell number for laboratory cultures and with cell-cycle based estimates of division rates for natural *Prochlorococcus* populations sampled near the beginning and end of the transect.

Estimated division rates of *Prochlorococcus* cultures. A non-axenic culture of *Prochlorococcus* MED4, a high-light adapted ecotype type I (eHLI), was grown in the laboratory at 20 ºC with a 16:8 light-dark cycle under 100 µE m^{-2} s^{-1} provided by white fluorescent tubes. Artificial seawater amended with Amp1 nutrients (6) was used as medium. The culture was grown in a 20-L batch culture for 2 days and analyzed with SeaFlow. To maintain stream stability and conserve culture volume over the span of the experiment, a peristaltic pump and tee union were used to combine a relatively low flow (1.5 mL min^{-1}) of the *Prochlorococcus* culture with a higher flow of artificial seawater in the SeaFlow instrument's sample line. The SeaFlow instrument then regulated the combined flow rate to 15 mL min^{-1} prior to measurement. Fluorescent microspheres (1 µm, Polysciences) were continuously injected for internal standards and alignment of the laser with the stream. *Prochlorococcus* cells were discriminated from bacteria according to their fluorescence characteristics.

6

To estimate division rate based on the size distribution, we estimated the parameters a, b, d_{max}, g_{max}, and E^* by fitting the model to hourly-averaged observations of the population size distribution over a 24-hr period using a 1-hr rolling window. Division rates therefore represent the average of 24 series of hourly division rates. The model parameters were subject to the following constraints $0 < d_{max} < 1$; $0 < g_{max} < 1$; $a > 0$; $b > 0$; $10 < E^* < 2000$, with E^* measured in µE m^{-2} s^{-1}.

In culture, the rate of change in cell abundance depends on the division rate and mortality rate:

$$\frac{dC}{dt} = \mu_{size}C - gC \qquad\qquad\qquad \text{[S6]}$$

where C is the hourly-averaged cell abundance, μ_{size} is the division rate based on the size distribution, g is the mortality rate. To calculate dC/dt, a third-order low-pass Butterworth filter (7) with a critical frequency set at 1/6 of the sampling rate was applied to C to dampen its variability (due to patchiness and instrument error). C was then realigned to account for phase shift due to filtering (Fig. S1A). Finally, hourly model-based division rates were compared to dC/dt. We found that g remained near 0 and μ_{size} was very similar to dC/dt (Fig. S1B), which indicates that the model provides good estimates of division rates for the *Prochlorococcus* culture ($R^2 = 0.76$, p < 0.001, Fig. S4A).

Estimated division rates based on cell cycle analysis. Two 28-hr time course experiments (October 29th, 2011 and October 31st, 2011) were conducted during the southward cruise in the sub-tropical Pacific gyre. Samples were collected every 2 hr from the continuous seawater flow-through system and fixed with 1% paraformaldehyde and 0.01% glutaraldehyde, stored in liquid nitrogen. Two months after sample collection, fixed samples were stained with 0.01% green-fluorescing DNA stain SYBR Green I (diluted with dimethylsulfoxide) for 15 minutes at room

temperature in the dark. Following the addition of fluorescent microspheres (1 μm, Polysciences) used as internal standard, stained samples were analyzed with a BD Influx flow cytometer. Data were obtained using the Spigot Operating Software version 5.0 (BD Biosciences) and analyzed using FlowJo version 9.7.2 (Tree Star). *Prochlorococcus* cells were discriminated from bacteria, cyanobacteria, and picoeukaryotes according to their light-scattering and fluorescence characteristics. A minimum of 10,000 *Prochlorococcus* cells was collected per sample. DNA frequency distributions were analyzed using FlowJo cell cycle platform to obtain cell fractions in G1, S, and G2+M phases.

In situ division rates based on DNA distributions (μ_{DNA}) were computed as described previously (8), based on the following equation:

$$\mu_{DNA} = \frac{1}{(n \times t_{S+G2+M})} \times \sum ln\,[1 + f_{s+G2+M}(i)] \tag{S7}$$

where n is the number of samples taken during the 24-hr period, t_{S+G2+M} combined duration of S and G2+M phases, and $f_{S+G2+M}(i)$ is the fraction of cells in S and G2+M for sample *i*. The duration of S and G2+M phases was estimated as twice the distance between the peak of cells in phase S and the peak of cells in the G2+M phase. The t_{S+G2+M} value was 8 hr and 6 hr for experiment performed at the beginning and the end of the cruise in the subtropical Pacific gyre, respectively, in agreement with previous studies in the subtropical North Pacific (8, 9).

Division rates based on measures of DNA content were compared to division rates based on the size-structured matrix population model (Fig. S2 and S3). The coefficients of determination $R^2 =$ 0.87 (p < 0.001) indicate that the division rate estimates from the model agree with those from DNA distributions (Fig. S4B).

8

Estimated division rates of *Prochlorococcus* in the field. The method used to estimate hourly division rates of *Prochlorococcus* in culture was applied to natural populations of *Prochlorococcus* in the field. Parameters fell into the following ranges: $0.008 < d_{max} < 0.551$; $0.005 < g_{max} < 0.997$; $7.77 < a < 14.99$; $1.43 < b < 3.79$; $56 < E* < 1999$ µE m^{-2} s^{-1}. In most cases, a fell into a relatively narrow range away from the constraints. Relaxing the constraints of a had a small effect on the estimated division rates and did not significantly change the projected size distribution.

Estimated mortality rates of *Prochlorococcus* in the field. In the Eulerian frame (i.e., at a fixed position), the rate of change in the abundance of *Prochlorococcus*, C, is a function of biological processes (i.e., division and mortality) and physical processes (i.e., advection and diffusion) which can either add or remove cells. The mass balance of C gives:

$$\frac{\partial C}{\partial t} = (\mu - g)C - u\frac{\partial C}{\partial x} + \kappa\frac{\partial^2 C}{\partial x^2} \qquad \text{[S8]}$$

where µ is the division rate, g is the mortality rate due to biological processes such as grazing and viral infection, C is the cell abundance, and u is the current velocity aligned along the axis of the ship's track, x, $\partial C/\partial x$ is the spatial gradient of C along the cruise track, and $\kappa\frac{\partial^2 C}{\partial x^2}$ is the mixing of C along the cruise track by the effective eddy diffusivity, κ.

The rate of change of C measured by the instrument from a moving ship is given by:

$$\frac{dC}{dt} = \frac{\partial C}{\partial t} + v_{ship}\frac{\partial C}{\partial x} \qquad \text{[S9]}$$

where v_{ship} is the velocity of the ship. Thus, the measured dC/dt reflects changes in C due to lo-

cal, time-dependent processes ∂C/∂t (e.g., biological and physical processes occurring at a particular location), and an advective component due to the ship moving through a spatial gradient of C, ∂C/∂x. We combine equation 8 and 9:

$$\frac{dC}{dt} = (\mu - g)C + (v_{ship} - u)\frac{\partial C}{\partial x} + \kappa\frac{\partial^2 C}{\partial x^2} \qquad \text{[S10]}$$

We neglect the current velocity, as $u \ll v_{ship}$. We also neglect the diffusive term, $\kappa\frac{\partial^2 C}{\partial x^2}$, as the estimated eddy diffusivity in the study region is very small (10). The mortality rate, gC, is thus given by:

$$gC = \mu C - \frac{dC}{dt} + v_{ship}\frac{\partial C}{\partial x} \qquad \text{[S11]}$$

We do not have a direct measure of ∂C/∂x, which is the spatial gradient of C along the cruise track for a fixed point in time. To approximate ∂C/∂x, we assumed that *Prochlorococcus* abundances remain constant from day to day at a given location (i.e., ∂C/∂t calculated over a 24-hr time interval is equal to 0), as observed from previous studies (11, 12) and during the first day on station (Fig. 2C, from day 1 to day 2). In this case, changes of the daily-averaged C along the cruise track are equal to v_{ship}∂C/∂x (see equation 9). Daily-averaged C was calculated using a 24-hr running mean of hourly-averaged C. The daily distance was calculated as the distance between the location at t0 and the location at t+24hr. A1-hr rolling window was then used to determine the start of each 24-hr period in the time series. A third-order low-pass Butterworth filter (7) with a critical frequency set at 1/6 of the sampling rate was applied to hourly-averaged C in order to dampen its variability (due to patchiness and instrument error). C was then realigned to account for phase shift due to filtering (Fig. S8A, B). The v_{ship}∂C/∂x term represented on average less than 25 % of total loss term and therefore played a secondary role in the observed patterns of cell mortality rates (Fig. S8C, D).

Idealized ecological models.

We used two different mathematical models that describe two-trophic-level microbial systems (i.e, virus/host and predator/prey systems) in continuous culture, based on our estimates of *Prochlorococcus* division rates.

We modeled the dynamics of host/virus interactions using the following system of equations, according to Levin's model (13):

$$\frac{dC}{dt} = \mu_t C - k_t CV - w(C - C_0)$$

$$\frac{dI}{dt} = k_t CV - (k_t C_{t-L} V_{t-L})e^{-wt} - wI$$

$$\frac{dV}{dt} = (bk_t C_{t-L} V_{t-L})e^{-wt} - k_t CV - mV - wV \qquad\qquad \text{[S12]}$$

where C represents the abundance of uninfected *Prochlorococcus* cells; I the abundance of infected cells; V the abundance of viruses; $\mu(t)$ the division rate of uninfected *Prochlorococcus* cells; $k(t)$ the per capita adsorption rate of the viruses; m the per capita mortality or decay rate of the viruses; w the washout rate; L and b the viral latent period and burst size, respectively; and the subscript $t - L$ indicates that the term is evaluated at a previous point in time. The initial conditions for the model were as follows: C=400 x 10^6 cells L^{-1} to represent *Prochlorococcus* abundance at the edge of the subtropical gyre; C_0 =400 x 10^6 cells L^{-1}, I=200 x 10^6 cells L^{-1}; V=1200 x 10^6 virus L^{-1}; w = 0.01 h^{-1}; m = 0.02 h^{-1} (based on decay rate of virus in unfiltered seawater) (14); L=8 hours and b=20 virions (corresponding to *Prochlorococcus* podovirus P-SSP7) (15, 16); μ(t) (h^{-1}) was defined as $\mu(t) = 0.015 \sin\left(\frac{2\pi t}{24} - \frac{\pi}{2}\right) + 0.02$, to represent hourly division rates of *Prochlorococcus* at the edge of the subtropical gyre (0.5 d^{-1}); $k(t)$ was set either as a constant (0.56 x 10^{-6} L h^{-1} cell^{-1}) (17) or defined as $k(t) = 0.56 \times 10^{-6}\left[\sin\left(\frac{2\pi t}{24} - \pi\right) + 0.5\right]$ to maximize adsorption during the peak of cells in S phase (2 hr before dusk) so the peak of

11

cell lysis would occur 6 hours after dusk, as observed *in situ*. Abundances were simulated for 100 days to reach a system at equilibrium. Under such a hypothetical scenario where viral lysis is the only source of *Prochlorococcus* cell mortality, the proportion of infected cells reach 50% of all cells when the system is at equilibrium (i.e., cell loss balances cell production over a daily cycle). Varying the initial number of infected cells (e.g., 1 % or 99% of all cells) changes the number of days required to reach equilibrium, but does not change the number of infected cells at equilibrium. Therefore, we arbitrarily set the number of infected cells at t0 to represent 50% of all cells.

The dynamics of the interactions between predator and prey can be modeled using Lokta-Volterra equations (18):

$$\frac{dC}{dt} = \mu_t C - a_t CP - w(C - C_0)$$

$$\frac{dP}{dt} = a_t CP - mP - wP \hspace{3cm} \textbf{[S13]}$$

where C represents the abundance of *Prochlorococcus* cells; P the abundance of predators; $\mu(t)$ the division rate of *Prochlorococcus* cells; $a(t)$ the per capita predation rate; m the per capita mortality rate of the predators; w the washout rate. The initial conditions for the model were as follows: $C = 400 \times 10^6$ cells L^{-1} to represent *Prochlorococcus* abundance at the edge of the sub-tropical gyre; $C_0 = 400 \times 10^6$ cells L^{-1}; $P = 40 \times 10^6$ cells L^{-1}; $w = 0.04$ h^{-1}; $m = 0.036$ h^{-1}; $\mu(t)$ (h^{-1}) was defined as $\mu(t) = 0.015 \sin\left(\frac{2\pi t}{24} - \frac{\pi}{2}\right) + 0.02$, to represent hourly division rates of *Prochlorococcus* at the edge of the subtropical gyre $(0.5$ $d^{-1})$; $a(t)$ was set either as a constant $(5.10^{-5}$ cell^{-1} $h^{-1})$ or defined as $a(t) = 5.10^{-5}\left[\left(1 + \sin\left(\frac{2\pi t}{24} - \pi\right)\right)\right]^2$ such that the predation rate was inversely correlated to irradiance. Abundances were simulated for 100 days to reach a system at

12

equilibrium.

***Prochlorococcus* qPCR.** High Light *Prochlorococcus* ecotype concentrations (eHL-I/eMED4 and eHL-II/eMIT9312) were determined by a qPCR assay as described previously **(19)**. Briefly, triplicate 100 mL samples were filtered on 0.22 μm polycarbonate filters using gentle vacuum (<100 mm Hg), followed by ~3 mL preservation solution (10 mmol L^{-1} Tris, 100 mmol L^{-1} EDTA, 0.5 mol L^{-1} NaCl) and stored at -80°C until later analysis. Cell lysates were made by shaking filters (≥ 4800 RPM) with 10 mmol L^{-1} Tris pH 8.0 in a bead beater without beads and the lysate incubated at 95°C for 15 min before being stored at -80°C until later analysis. qPCR protocols, based on primers and conditions specific for a given clade of *Prochlorococcus* and calibrated with cultures, utilized Sybr I Green to quantify amplicons. For each run, the purity of products was evaluated and verified using dissociation curve analyses.

References

1.   Swalwell JE, Ribalet F, Armbrust EV (2011) SeaFlow: A novel underway flow-cytometer for continuous observations of phytoplankton in the ocean. *Limnology and Oceanography: Methods* 9:466–477.

2.   Ribalet F, Schruth DM, Armbrust EV (2011) flowPhyto: enabling automated analysis of microscopic algae from continuous flow cytometric data. *Bioinformatics* 27:732–733.

3.   Sosik HM, Olson RJ, Neubert MG, Shalapyonok A, Solow AR (2003) Growth Rates of Coastal Phytoplankton from Time-Series Measurements with a Submersible Flow Cytometer. *Limnology and Oceanography* 48:1756–1765.

4.   Hunter-Cevera KR et al. (2014) Diel size distributions reveal seasonal growth dynamics of a coastal phytoplankter. *Proceedings of the National Academy of Sciences* 111:9852–9857.

5.   Mullen KM, Ardia D, Gil DL, Windover D, Cline J (2011) DEoptim: An R Package for Global Optimization by Differential Evolution. *J Stat Softw* 40:1–26.

6.   Moore LR et al. (2007) Culturing the marine cyanobacterium *Prochlorococcus*. *Limnolo-*

gy and Oceanography: Methods 5:353–362.

7. Roberts J, Roberts TD (1978) Use of the Butterworth low-pass filter for oceanographic data. *J Geophys Res* 83:5510.

8. Liu H, Nolla H, Campbell L (1997) *Prochlorococcus* growth rate and contribution to primary production in the equatorial and subtropical North Pacific Ocean. *Aquatic Microbial Ecology* 12:39–47.

9. Worden A, Binder B (2003) Application of dilution experiments for measuring growth and mortality rates among *Prochlorococcus* and *Synechococcus* populations in oligotrophic environments. *Aquatic Microbial Ecology* 30:159–174.

10. Abernathey RP, Marshall J (2013) Global surface eddy diffusivities derived from satellite altimetry. *Journal of Geophysical Research-Oceans* 118:901–916.

11. Vaulot D, Marie D (1999) Diel variability of photosynthetic picoplankton in the equatorial Pacific. *Journal of Geophysical Research C Oceans* 104:3297–3310.

12. Cavender-Bares K, Mann E, Chisholm S, Ondrusek M, Bidigare R (1999) Differential Response of Equatorial Pacific Phytoplankton to Iron Fertilization. *Limnology and Oceanography* 44:237–246.

13. Levin BR, Stewart FM, Chao L (1977) Resource-Limited Growth, Competition, and Predation: A Model and Experimental Studies with Bacteria and Bacteriophage. *The American Naturalist* 111:3–24.

14. Suttle CA, Chen F (1992) Mechanisms and rates of decay of marine viruses in seawater. *Applied and Environmental Microbiology* 58:3721–3729.

15. Lindell D, Jaffe JD, Johnson ZI, Church GM, Chisholm SW (2005) Photosynthesis genes in marine viruses yield proteins during host infection. *Nature* 438:86–89.

16. Lindell D et al. (2007) Genome-wide expression dynamics of a marine virus and host reveal features of co-evolution. *Nature* 449:83–86.

17. Avrani S, Wurtzel O, Sharon I, Sorek R, Lindell D (2011) Genomic island variability facilitates *Prochlorococcus*–virus coexistence. *Nature* 474:604–608.

18. Lokta AJ (1920) Analytical note on certain rhythmic relations in organic systems. *Proceedings of the National Academy of Sciences of the United States of America* 6:410–415.

19. Lin Y et al. (2013) In situ activity of a dominant *Prochlorococcus* ecotype (eHL-II) from rRNA content and cell size. *Environmental Microbiology* 15:2736–2747.

20. Johnson ZI et al. (2006) Niche Partitioning Among *Prochlorococcus* Ecotypes Along Ocean-Scale Environmental Gradients. *Science* 311:1737–1740.

21. Moore L, Goericke R, Chisholm SW (1995) Comparative physiology of *Synechococcus* and *Prochlorococcus*: influence of light and temperature on growth, pigments, fluorescence and absorptive properties. *Marine Ecology Progress Series* 116:259–275.

22. Moore L, Chisholm S (1999) Photophysiology of the marine cyanobacterium *Prochlorococcus*: Ecotypic differences among cultured isolates. *Limnology and Oceanography* 44:628–638.

23. Burbage CD, Binder BJ (2007) Relationship between cell cycle and light-limited growth rate in oceanic *Prochlorococcus* (MIT9312) and *Synechococcus* (WH8103) (Cyanobacteria). *Journal of Phycology* 43:266–274.
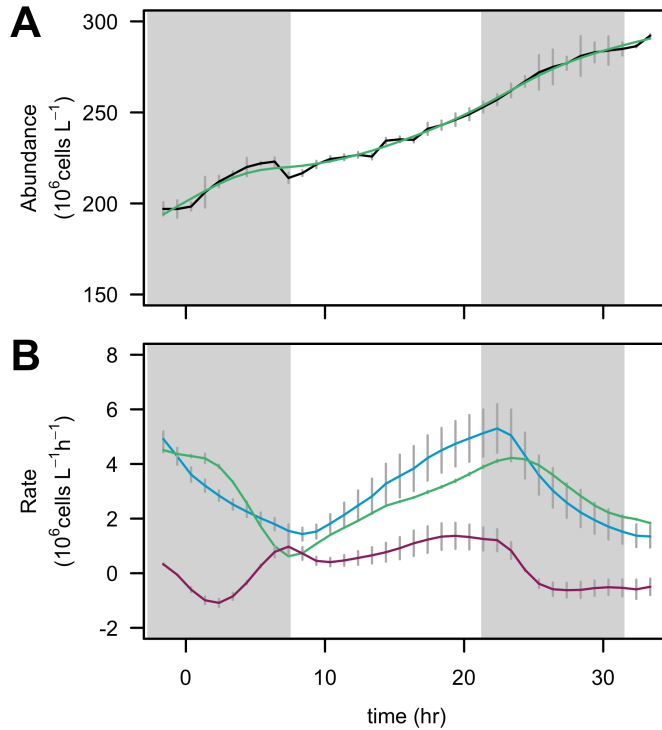
Fig. S1: Validation of the size-based division rate model with cultured isolate. A) Hourly-averaged *Prochlorococcus* (MED4) cell abundances (10^6 cells L^{-1}, C, black line). A low-pass filter was applied to C in order to dampen its variability (C$_{lp}$, green line). B) Hourly rates (10^6 cells L^{-1} h^{-1}) of change in C$_{lp}$ (dC$_{lp}$/dt, green line), estimates of cell production (μ_{size}C, blue line) and cell mortality (gC, purple line, calculated from the difference between μ_{size}C and dC$_{lp}$/dt). The grey regions indicate night. Vertical grey bars represent standard deviations (n=20 for abundances, n=24 for the rates).
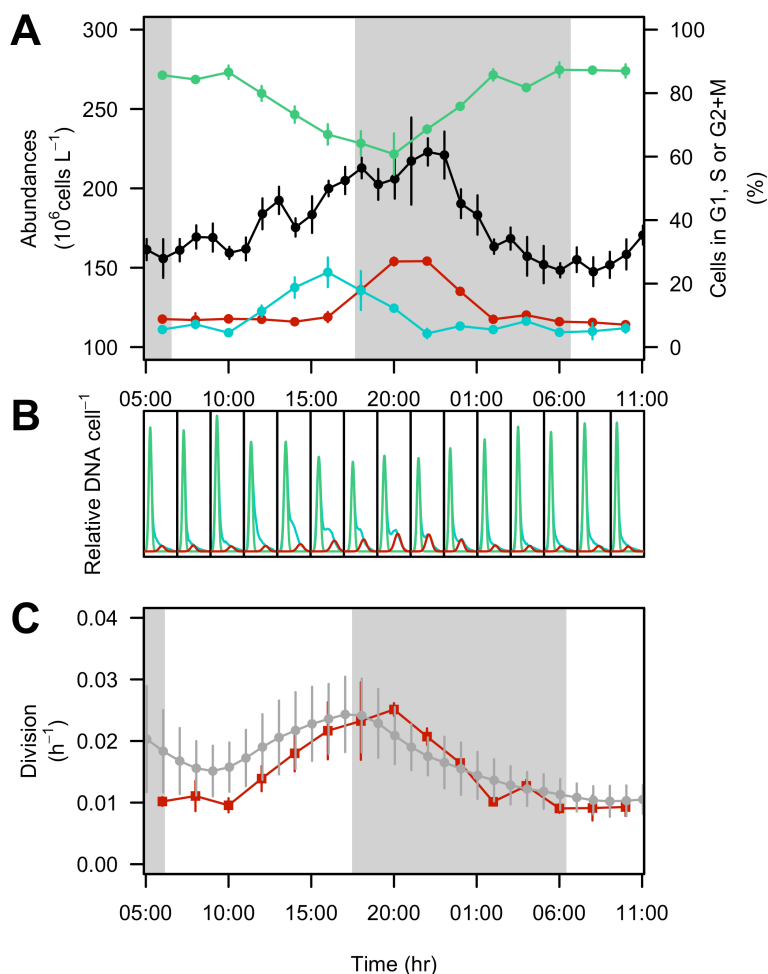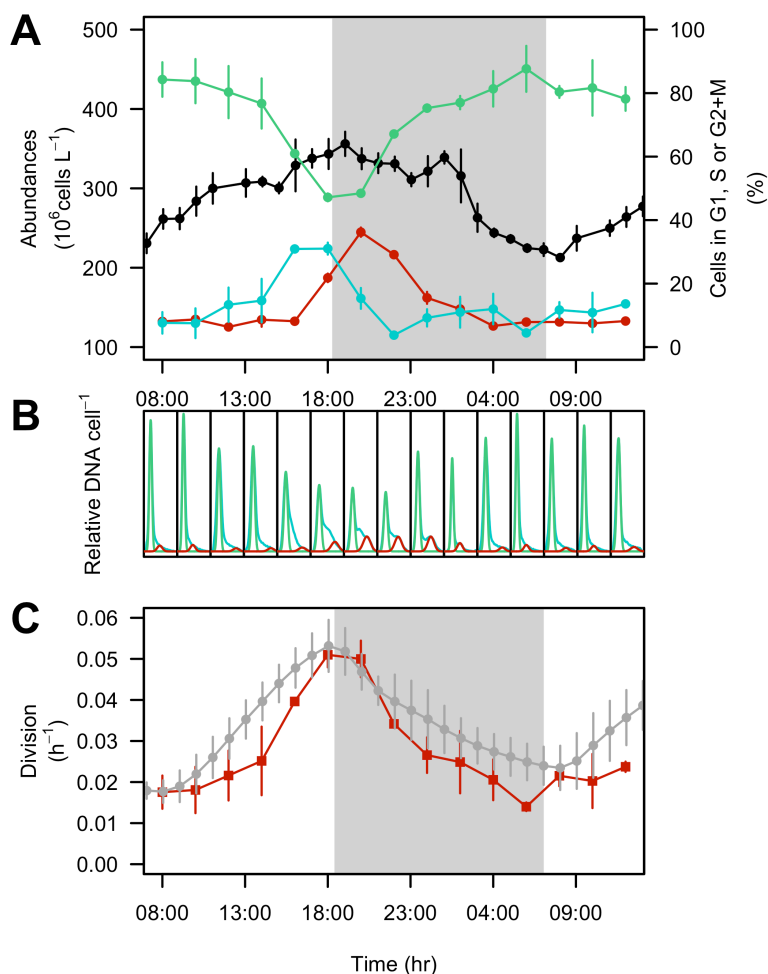
Fig. S2: *Prochlorococcus* **division pattern** *in situ* (October 29th, 2011). A) Cell abundances (10^6 cells L^{-1}, black line) and percentage of cells in G1 (green line), S (blue line) and G2+M (red line) phases. B) DNA frequency distributions of cells (relative DNA cell^{-1}) in G1 (green line), S (blue line) and G2+M (red line) phases. C) Hourly division rates (h^{-1}) based on the relative proportions of cells in S+G2+M phases (red line) and based on the size distribution (grey line). The grey regions indicate night. Vertical bars represent standard deviations (n=20 for abundances, n=3 for the percent of cells in G1, S and G2+M phases, n=24 for the size-based division rates).

**Fig. S3:** *Prochlorococcus* **division pattern** *in situ* (October 31st, 2011). A) Cell abundances (10^6 cells L^{-1}, black line) and percentage of cells in G1 (green line), S (blue line) and G2+M (red line) phases. B) DNA frequency distributions of cells (relative DNA cell^{-1}) in G1 (green line), S (blue line) and G2+M (red line) phases. C) Hourly division rates (h^{-1}) based on the relative proportions of cells in S+G2+M phases (red line) and based on the size distribution (grey line). The grey regions indicate night. Vertical bars represent standard deviations (n=20 for abundances, n=3 for the percent of cells in G1, S and G2+M phases, n=24 for the size-based division rates).

18
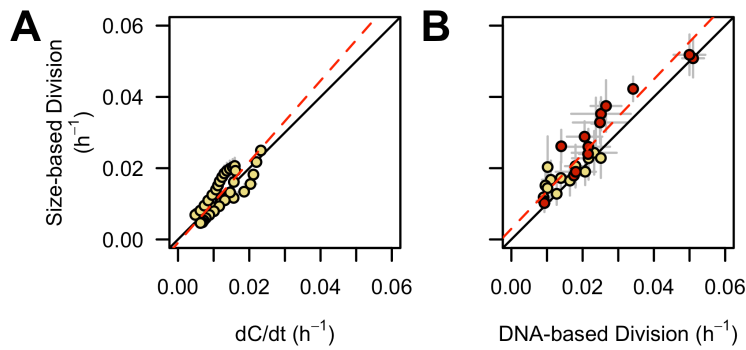
Fig. S4: Comparison of division rate estimates based on size-structured matrix population model with other methods. A) Comparison of size-based division rates (h^{-1}) with the hourly rates of change in cell abundances in *Prochlorococcus* culture (MED4) (dC/dt, h^{-1}). B) Comparison of size-based division rates (h^{-1}) of *Prochlorococcus* in the field with those based on cell-cycle based division rates estimated during two 28-hr experiments at the beginning (yellow, October 29th, 2011) and end (red, October 31st, 2011) of the transect. Red lines represent the linear model II regression ($R^2 = 0.76$, p< 0.001, and $R^2 = 0.87$, p< 0.001, for laboratory and field experiments, respectively); black line represents the 1:1 relationship.
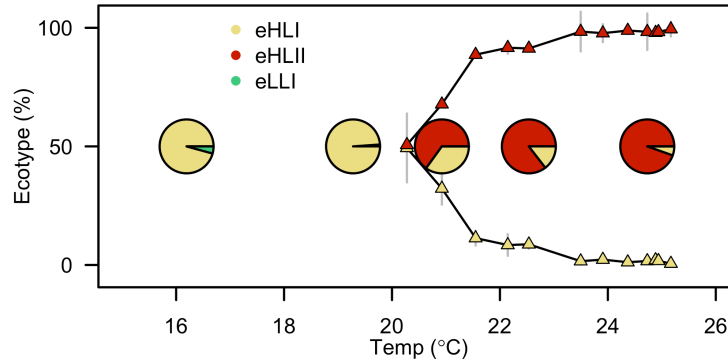
Fig. S5: *Prochlorococcus* ecotype composition along the temperature gradient. Pie charts are based on percent of each *Prochlorococcus* ecotype relative to total *Prochlorococcus* ecotypes represented in 16S rRNA gene amplicons; triangles represent the percent of eHLI / eHLII ecotypes determined by qPCR. Yellow, red and green colors represent eHLI, eHLII and eLLI ecotype, respectively. Vertical grey bars represent standard deviations (n=3).
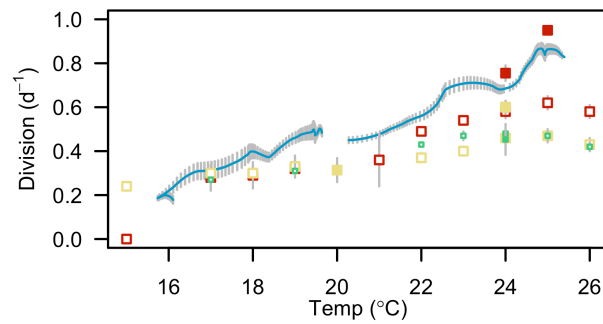
Fig. S6: Relation between daily division rates (d⁻¹) of *Prochlorococcus* and temperature (ºC). Daily division rates (d⁻¹) of *Prochlorococcus* during the survey (blue line) and from high-light adapted ecotype I and II (eHLI and eHLII) and low-light adapted ecotype I (eLLI) grown in culture at different temperatures under low light exposure (66 µE m⁻² s⁻¹, 14:10 LD cycle) (yellow, red and green open squares for eHLI, eHLII and eLLI ecotype, respectively) (20), and under high light exposures (from 70 to 300 µE m⁻² s⁻¹, 14:10 LD cycle) at 20 ºC (21, 22), 24 ºC (23) and 25 ºC (this study, see Supplemental Information) (yellow, red and green closed squares for eHLI, eHLII and eLLI ecotype, respectively). Daily division rates during the survey were calculated using a 24-hr running mean of hourly size-based division rates. Vertical grey bars represent standard deviations (n=24 for size-based division rates, n > 3 for the culture studies).
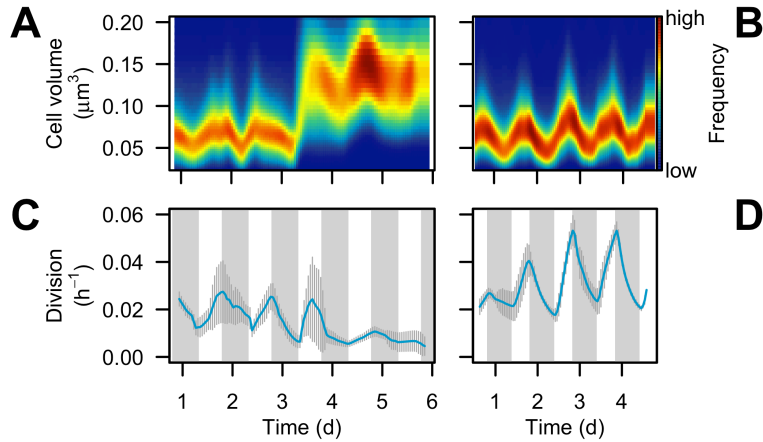
Fig. S7: Estimates of *Prochlorococcus* size distribution and size-based division rates during the survey. A, B) *Prochlorococcus* size distribution (μm^3) estimated by SeaFlow. C, D) Hourly estimates of division rates (blue line) during the northward cruise to California (October 4th – 9th, 2011) and southward cruise to Hawaii (October 29th – November 2nd, 2011) (left and right panel, respectively). Vertical grey bars represent the standard deviation of size-based division rates (n=24); the grey regions indicate night. Note: a ~ 3 fold change in cell volume (panel a) over day 3 was observed during the transect between stations on the northward cruise and precluded accurate estimates of division rate during this period.
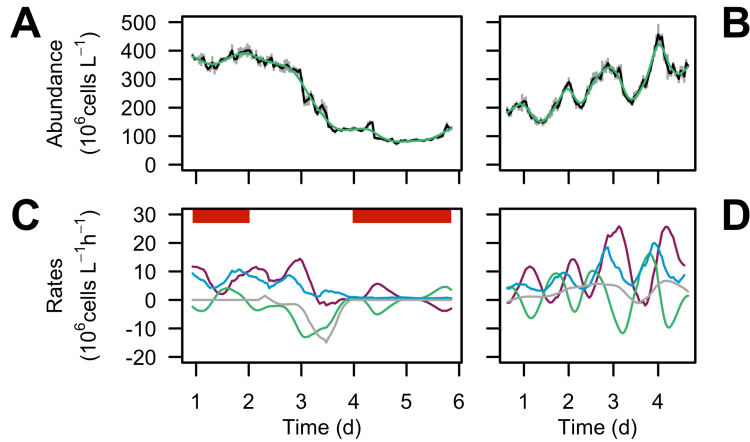
Fig. S8: Estimations of mortality rates of *Prochlorococcus* in the field. A, B) Hourly-averaged *Prochlorococcus* cell abundances (10^6 cells L^{-1}, C, black line) measured by SeaFlow. A low-pass filter was applied to C in order to dampen its variability (C_{lp}, green line). C, D) Hourly rates (10^6 cells L^{-1} h^{-1}) of change in C_{lp} (dC/dt, green line), estimates of cell production ($\mu_{size}C$, blue line), hourly rates of change in C_{lp} due to physical transport ($v_{ship}\partial C_{lp}/\partial x$, grey line) and net population loss rates (gC, purple line) (see equation 11 in Supplemental Information for details) during the northward cruise to California (October 4th – 9th, 2011) (left panels) and southward cruise to Hawaii (October 29th – November 2nd, 2011) (right panels). Vertical grey bars represent the standard deviation of hourly-averaged cell abundances (n=20). Horizontal red bars represent periods on station.
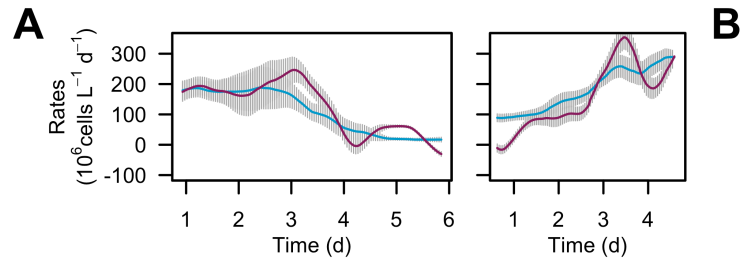
Fig. S9: Comparison of daily *Prochlorococcus* cell production and cell mortality during the survey. A, B) Daily rates of cell production (10^6 cells L^{-1} d^{-1}, blue line) and cell mortality (10^6 cells L^{-1} d^{-1}, purple line) during the northward cruise to California (October 4th – 9th, 2011) (A) and southward cruise to Hawaii (October 29th – November 2nd, 2011) (B). Daily rates were calculated as the sum of hourly estimates of cell production and cell mortality rates over a 24-hr period using a 1-hr rolling window. Vertical grey bars in represent standard deviations (n=24).
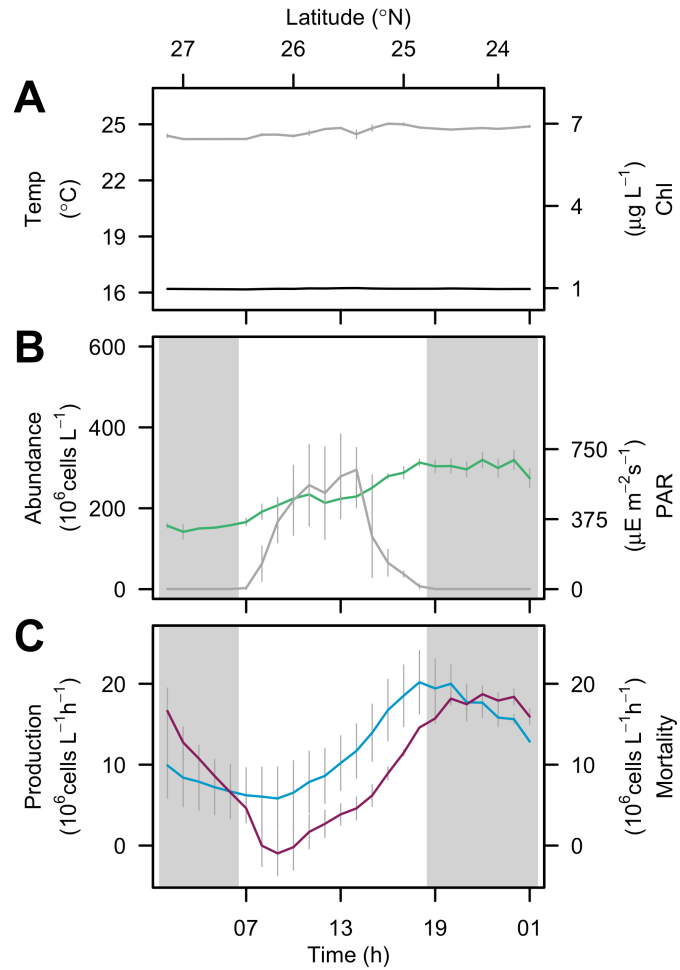
Fig. S10. Conserved diel patterns in the Pacific gyre in winter. (A) Hourly-averaged tempera-

ture (°C, grey line) and bulk chlorophyll *a* concentrations (μg L⁻¹, black line), (B) hourly-

averaged cell abundances (10^6 cells L⁻¹, green line) and hourly-averaged PAR at 5 m depth (μE

m⁻² s⁻¹, grey line), (C) hourly rates of cell production (10^6 cells L⁻¹ h⁻¹, blue line) and cell mortali-

ty (10^6 cells L⁻¹ h⁻¹, purple line) during the southward cruise to Hawaii (November 16th – 17th,

2010). Vertical grey bars represent standard deviations (n=20 for temperature, chlorophyll *a* con-

centrations, PAR and cell abundances, n=24 for cell production and mortality rates). The grey
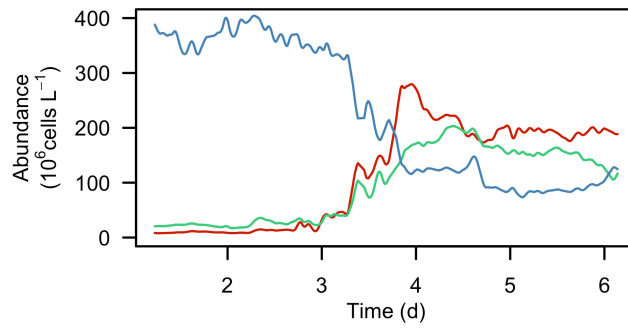
regions indicate night.

Fig. S11: Distribution of phytoplankton populations at the edge of the North Pacific gyre.
Cell abundances (10^6 cells L^{-1}) of *Prochlorococcus* (blue line), *Synechococcus* (red line) and picoeukaryote phytoplankton (green line) during the northward cruise to California (October 4th – 9th, 2011).